Appl Phys A (2010) 98: 407–415
DOI 10.1007/s00339-009-5405-x

Applied Physics A
Materials Science & Processing

Modeling of multi-burst mode pico-second laser ablation for improved material removal rate

Wenqian Hu · Yung C. Shin · Galen King

Received: 8 May 2009 / Accepted: 20 August 2009 / Published online: 17 September 2009

Abstract This paper deals with the unique phenomena occurring during the multi-burst mode picosecond (ps) laser ablation of metals through modeling and experimental studies. The two-temperature model (TTM) is used and expanded to calculate the ablation depth in the multi-burst mode. A nonlinear increment of ablation volume is found during the multi-burst laser ablation. The deactivation of ablated material and the application of temperature-dependent electron-phonon coupling are demonstrated to be important to provide reliable results. The simulation results based on this expanded laser ablation model are experimentally validated. A significant increase of ablation rate is found in the multi-burst mode, compared with the single-pulse mode under the same total fluence. This numerical model provides a physical perspective into the energy transport process during multi-burst laser ablation and can be used to study the pulse-to-pulse separation time effect on the ablation rate.

PACS 61.20.Lc · 63.20.kd · 64.60.A · 42.62.Cf · 44.10.+i

1 Introduction

Ultrashort pulse laser ablation is capable of producing high-quality micro features on different kinds of materials with precise material removal, small heat-affected zones (HAZ), and reduced thermal damage, owing to the short pulse duration τ_d [1–3]. However, the ablation depth is usually limited due to the shallow penetration depth per pulse [2–4] when laser fluence near the ablation threshold is used. On the other hand, if a higher fluence way above the ablation threshold is applied, thermal damage will be induced into the material or burrs will be generated on the surface [5]. Therefore, in order to increase the ablation depth with normal laser fluence, multi-burst mode laser ablation has been investigated in place of single-pulse mode [4–7].

In multi-burst mode laser ablation, at least two pulses are generated within a very short period, with the pulse-to-pulse separation time τ_s usually below 1 μs. This type of laser ablation has also been investigated to enhance x-ray line emission from plasmas [8], in addition to process quality improvement and ablation rate enhancement, mentioned above.

However, for multi-burst mode laser ablation of metal with ultrashort pulses, ablation rate is not always enhanced as compared to single-pulse mode. This process is distinct from previous work on double-pulse machining with longer pulse duration (microsecond or nanosecond (ns)), either of which use the second pulse to drive away the melt pool produced by the first pulse [9] or use the debris generated by the first pulse in a timely manner for further etching [10]. In multi-burst mode ultrashort laser ablation, the pulse-to-pulse separation time τ_s, which varies from sub-ps to ns, will result in different regimes [4–6, 11] of the laser-metal interaction for lasers with focal spot diameters around 10 μm under ambient atmosphere. This is due to the different significance of plasma shielding and heat accumulation, which two have contradictory effects on the enhancement of the ablation rate [12]. Therefore, the physical ablation mechanism in the multi-burst mode needs to be better understood. This study focuses on the case with τ_s short enough to constrain heat accumulation between the pulses while long enough to avoid plasma shielding.

W. Hu · Y.C. Shin (✉) · G. King
Center for Laser-based Manufacturing, School of Mechanical Engineering, Purdue University, West Lafayette, IN 47907, USA
e-mail: shin@purdue.edu
Fax: +1-765-4940539

TTM is extensively used to examine the ablation characteristics of material with single ultrashort laser pulse [13–15] and multi-burst mode ablation with a linear relationship [7]. Different from [7], material temperature evolutions and corresponding property changes during pulse irradiation time as well as pulse-to-pulse separation time are emphasized in this study. Interaction between ablated material and unablated material is also considered. The validity of this model will be discussed by comparison with experimental results.

2 Experimental setup

The laser system used for this study consists of a ps Nd:YVO_4 laser (Lumera RAPID), with average power $P = 2$ W, pulse duration $\tau_d = 10$ ps (full width at half maximum, FWHM), and repetition rate ranging from 10 to 500 kHz. Laser pulses can be generated on demand, for example, with tailored user-defined pulse trains, or bursts. The burst consists of a certain number of pulses with $\tau_d = 10$ ps and $\tau_s = 20$ ns, as shown in Fig. 1. The maximum number of pulses in a burst depends on the repetition rate.

Laser percussion drilling with the fundamental wavelength (1064 nm) was performed on Cu at repetition rates of 100 kHz, 50 kHz, and 10 kHz using this laser system. An optical surface profilometer (ADE MicroXAM) was utilized to measure ablation depths and three-dimensional profiles of drilled holes, which were used for the calculation of ablation volumes.

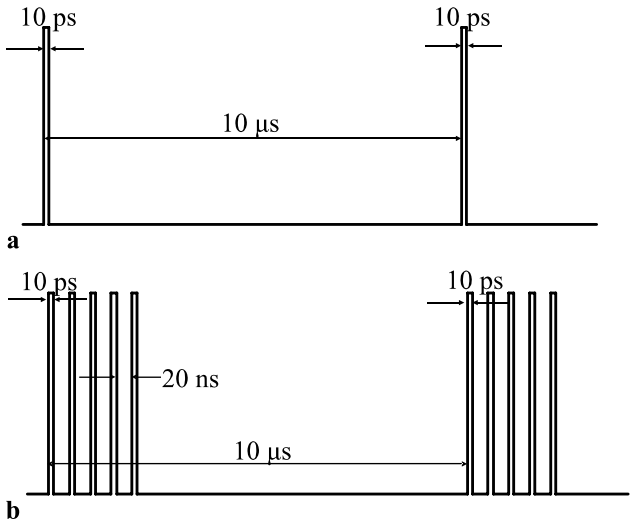

Fig. 1 Schematic diagrams of laser pulse temporal profiles with pulse duration $\tau_d = 10$ ps (FWHM) and repetition rate of 100 kHz. (**a**) Single-pulse mode where the pulse-to-pulse separation time τ_s is 10 µs. (**b**) Multi-burst mode where τ_s within a burst is 20 ns

3 Multi-burst laser ablation model

The schematic of the simulation domain is illustrated in Fig. 2. At the beginning of the ablation process, the laser pulse irradiates the left surface of the material at coordinate $z = 0$ nm. The right surface at $L = 10000$ nm denotes the bottom of the simulation domain, where the constant temperature (300 K) boundary condition is applied. Initial temperatures of electrons and the lattice in all grids are set at $T_0 = 300$ K. Each grid represents a couple of material layers.

A simplified TTM-based model [14], which can predict the ablation depth of a single pulse for metal with reasonable accuracy and is computationally feasible for a simulation domain with spatial depth up to 10 µm and temporal length up to 100 ns, was used and expanded in this study. The main features of this simplified model, instead of the detailed description, are discussed in this section.

It was suggested that the critical point phase separation (CPPS) is the dominant physical mechanism for material removal during ultrashort laser ablation of metals at high fluences (around 0.6–1 J/cm^2) [16]. The material layer whose expansion trajectory enters the unstable zone near the critical point is defined as the separation point. The depth of the separation point can be adequately regarded as and represented by the depth of ablation, d_i, as denoted in Fig. 2. The maximum temperature that the separation point reaches is called the separation temperature T_{sep}, and expressed as [14]

$$T_{\text{sep}} = T_c \left(\frac{\rho_0}{\rho_c} \right)^{2/3} \tag{1}$$

where ρ_0, ρ_c, and T_c are the normal density, critical density, and critical temperature, respectively.

The instantaneous location of the separation point is calculated by using TTM [17]:

$$C_e \frac{\partial T_e}{\partial t} = \frac{\partial}{\partial z} \left(k_e \frac{\partial T_e}{\partial z} \right) - G(T_e - T_i) + S \tag{2}$$

$$C_i \frac{\partial T_i}{\partial t} = G(T_e - T_i) \tag{3}$$

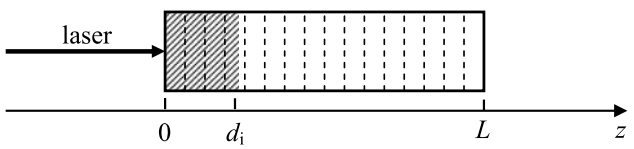

Fig. 2 A schematic diagram of the simulation domain. The laser pulse irradiates the left surface of the material and z denotes the laser irradiation direction. Domain depth $L = 10000$ nm. d_i denotes the instantaneous ablation depth. A few coarse grids, instead of fine grids used in simulation, are shown for clarity

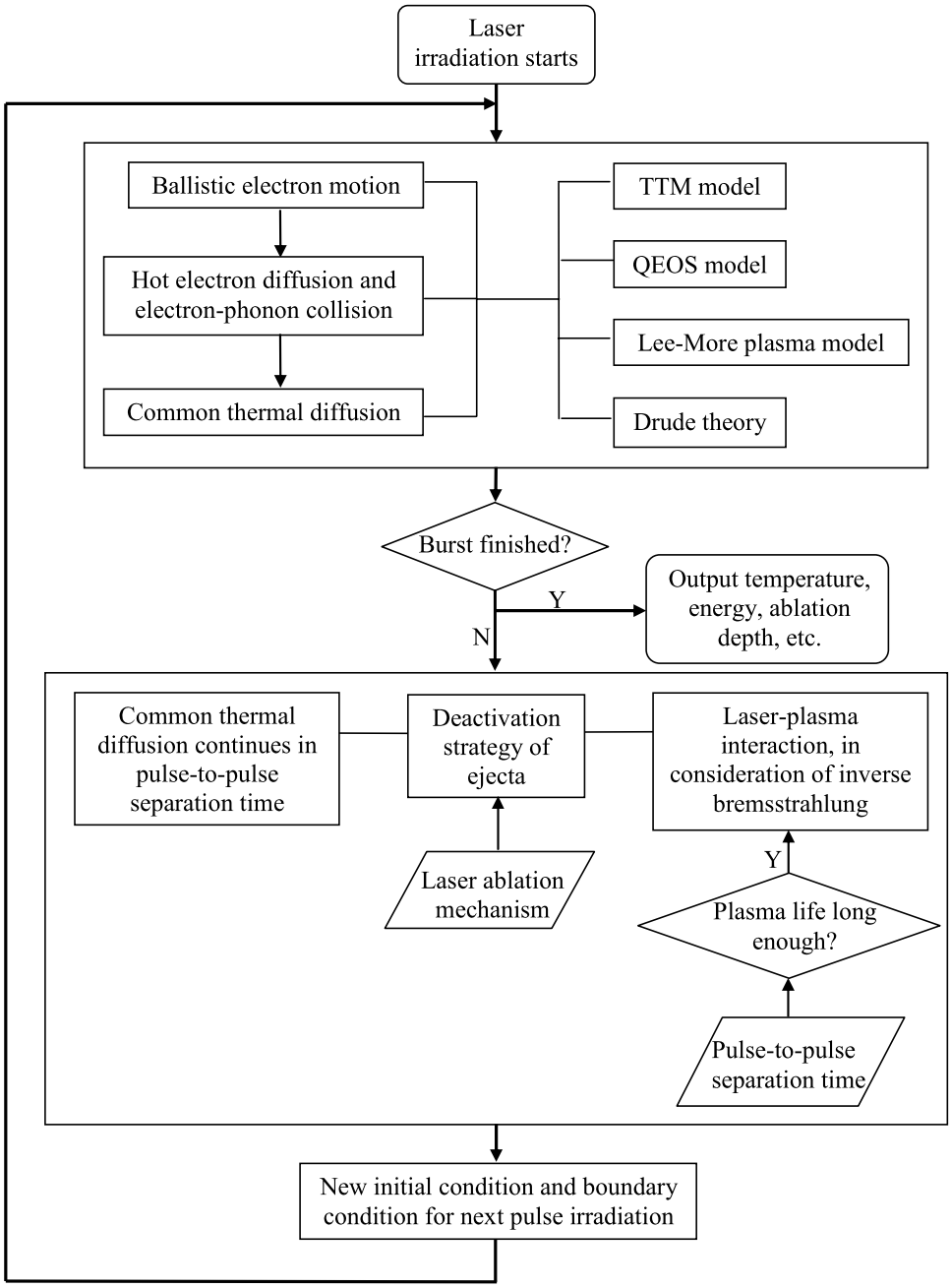

Fig. 3 A schematic diagram of the physical phenomena and corresponding numerical models used in multi-burst mode laser ablation

where T_e, T_i, C_e and C_i are the temperatures and the volumetric heat capacities of electrons and the lattice, respectively, k_e is the electron thermal conductivity, G is the electron-phonon coupling, and S is the laser energy source term.

The auxiliary equations needed to solve (2) and (3) are given by (4) and (5):

$$G = C_e/\tau_\varepsilon \tag{4}$$

$$S = (1 - R)\alpha I \exp(-\alpha z) \tag{5}$$

where τ_ε is the mean energy exchange time for electrons and the lattice, i.e., the electron relaxation time, R is the surface reflectivity, α is the absorption coefficient, and I is the laser power density reaching the target surface. Material properties in (2)–(5) are obtained by using QEOS model, Lee-More plasma model, and Drude theory as discussed in [14].

For the multi-burst mode laser ablation, additional physical phenomena and corresponding numerical models are schematically demonstrated in Fig. 3. The simulation domain is the same as that of the single-pulse laser ablation

model (Fig. 2). First of all, during the pulse-to-pulse separation time, electrons and the lattice are either about to reach, or already at thermal equilibrium ($T_e = T_i = T$) and the laser source term becomes zero. Therefore, the two equations (2) and (3) can be rewritten as one,

$$(C_e + C_i)\frac{\partial T}{\partial t} = \frac{\partial}{\partial z}\left(k_e \frac{\partial T}{\partial z}\right) \tag{6}$$

The common thermal diffusion continues to drive the heat dissipation from the hotter surface to the deeper and colder region of the material. On the other hand, the energy loss through the free surface of ablated material will be much less compared with interior diffusion.

Second, the lifetime of the plasma produced during laser ablation determines whether or not the interaction of the plasma with succeeding pulses should be considered. Reference [18] proposes a formula to calculate the time during which the ablation occurs and the plasma forms. The calculated time period is on the order of sub-ns for Cu. Specifically, no further evolution of the plasma volume is observed after 25 ns for the plasma induced on Cu with a 10 ps laser at a pulse energy of 20 μJ [19]. If this laser energy is decreased, the temporal evolution of the longitudinal Cu plasma is shown to discontinue much sooner [20]. Therefore, it can be reasonably assumed that for the 10 ps laser used in this study, with the pulse energy lower than 13 μJ or laser fluence in the range of 0–4 J/cm^2 (with diameter of hole 20 μm), the plasma shielding effect can be neglected after 20 ns.

The third issue is the interaction of the ablated material and the unablated material. If CPPS occurs, the thermodynamic trajectories of the ablated material layers will follow approximately the adiabat for perfect gases [16], which means there is no energy exchange between those ejecta and the unablated material. To account for this phenomenon in the model, a method of eliminating the ablated material (grids in simulation domain) as shown by the shaded region in Fig. 2, was proposed and applied in this study. The grids that have been ablated by previous pulses have to be redefined as completely inactive by setting their thermal conductivities to zero. Meanwhile, a new boundary needs to be specified for the remaining active grids, which means that the zero point of the variable z in (5) has to be redefined from 0 to current ablation depth d_i. Most of the laser energy is absorbed at the new boundary since the absorption decreases exponentially with depth z in the material. To reduce the errors resulting from the numerical discretization method, either the mesh has to be refined or the grids have to be partially deactivated.

The simulated advancement of the ablation depth with five successive pulses in a burst (5-burst mode) at laser fluence $F = 2$ J/cm^2 (per pulse) is shown in Fig. 4. The number of pulses is set at five for the burst, because it provides high enough laser energy per pulse if same total fluence is applied and also generates significant performance difference from the single-pulse mode. The diameter of the hole, D, is 20 μm, and the individual ablation depth by each pulse is 51.3 nm, 56.3 nm, 61.0 nm, 65.5 nm and 68.9 nm. The increase of ablation depths for latter pulses in the same burst demonstrates a nonlinear laser-material interaction, primarily due to the effect of local heating from former pulses. This nonlinear interaction distinguishes this model from previous work [7], where the ablation depth is the same for each pulse in a burst.

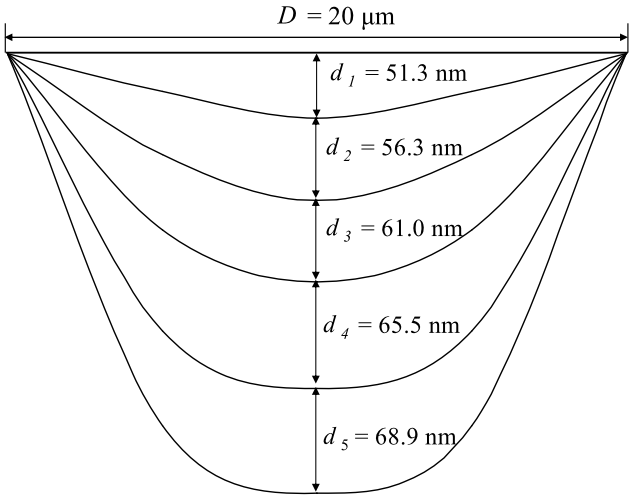

Fig. 4 A schematic diagram of the ablation depth evolvement with five successive pulses (laser fluence $F = 2$ J/cm^2, hole diameter $D = 20$ μm). The ablation depths d_1 to d_5, representing the individual ablation depth by the first to the fifth pulses, are obtained from simulation results

This local heating effect, or energy accumulation between pulses, is illustrated by simulation results, as shown in Figs. 5 to 7. Figure 5 shows the simulation of the material temperature vs. grid position at different instantaneous time from 10 ps to 20 ns. After the first pulse irradiation, a certain amount of material layers near the left surface have been ablated, and others next to the ablated layers have been heated up to a very high temperature as shown by the dashed curve (20 ps). During the pulse-to-pulse separation time, electrons and the lattice are at thermal equilibrium and the heat is continuously diffused into deeper material layers, as shown by these three curves (100 ps, 1 ns, and 20 ns). Finally, the surface lattice temperature reaches about 1000 K before the irradiation of the second pulse and a local high temperature zone, depth of about 1000 nm, is created, denoted by the dash dot curve (20 ns) in Fig. 5. It is important to note that this local temperature zone with $F = 2$ J/cm^2 is still small as compared to the thermal damage zone (deeper than 5000 nm) generated by the 25-ns laser ablation with $F = 0.13$ J/cm^2 [21].

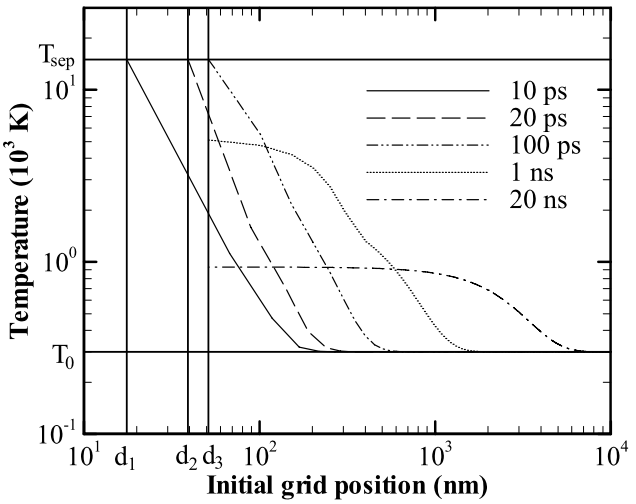

Fig. 5 The simulated evolvement of material temperature during one pulse laser ablation at different instantaneous time from 10 ps to 20 ns, where initial temperature $T_0 = 300$ K, separation temperature $T_{sep} = 15000$ K, and instantaneous ablation depths $d_1 = 17.5$ nm, $d_2 = 39.2$ nm, $d_3 = 51.3$ nm. The laser beam irradiates at the left surface of the material with laser fluence $F = 2$ J/cm^2

The local heating effect from former pulses leads to the change of temperature, and thus the change of transport properties of the material. The application of temperature-dependent transport properties is important of obtaining accurate results [22]. Figure 6(a) shows that the electron relaxation time τ_ε decreases by about 70%, whereas the electron-phonon coupling factor G increases by 11 times from $T_e =$ 300 K to $T_e = 1000$ K. The diffusive energy will be transported by hot electrons during the electron relaxation time, beyond which the common thermal diffusion dominates and replaces the hot electron diffusion. The coupling between electrons and phonons is strengthened with a shorter relaxation time and contributes to a higher energy transfer rate from electrons to the lattice, as shown in Fig. 6(b). These results are all owing to the energy accumulation between pulses. Similarly, because the initial material boundary for the second laser pulse irradiation has a higher temperature, the ablation depth is increased as compared with the first laser pulse.

The local heating effect is also illustrated by the evolvement of the left boundary temperature plotted in Fig. 7. Each pulse ablation has a distinct left boundary at the surface where the laser irradiates, because this surface is shifted toward right after material is ablated, as shown in Fig. 2. The boundary temperature jumps up sharply during the period of laser irradiation, and then falls down gradually by transporting heat to the deeper material. The initial boundary for the latter pulse ablation has a higher temperature than that for the previous one, increasing from 300 K for the first pulse to 3066.3 K for the fifth pulse. For the latter pulses, electrons have a higher temperature at the beginning of the

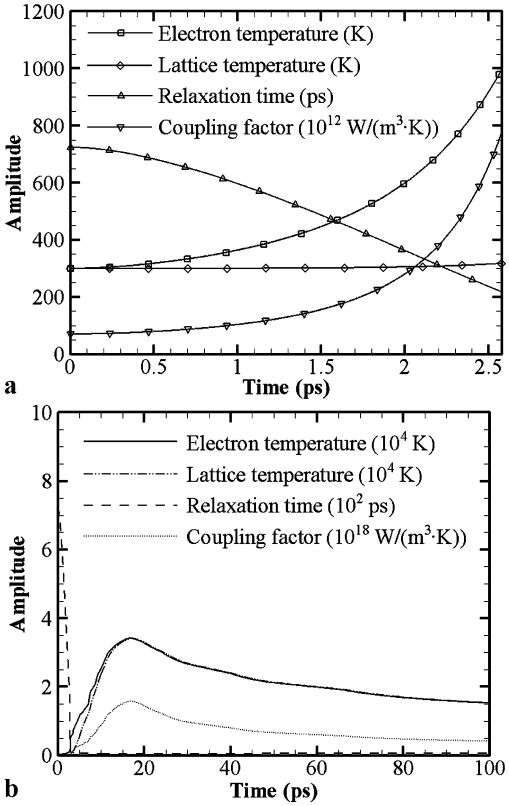

Fig. 6 Simulated developments of the temperatures of electrons (T_e) and the lattice (T_i) as well as the relaxation time (τ_ε) and the electron-phonon coupling factor (G) during one pulse laser ablation. (**a**) Plotted on a short time scale, where T_e rises up from 300 K to 1000 K within 2.58 ps, while τ_ε drops from 723.5 ps to 217.2 ps, and G increases from 70.5×10^{12} W/(m^3·K) to 781.9×10^{12} W/(m^3·K). (**b**) Plotted on a long time scale, where T_i jumps up, as soon as τ_ε falls down to about 5 ps. The laser pulse begins to irradiate at 0 ps with laser fluence $F = 2$ J/cm^2

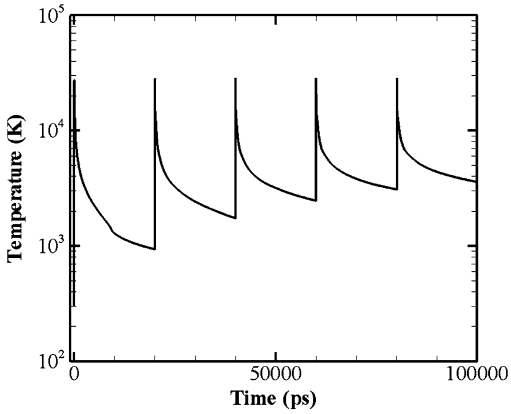

Fig. 7 Simulated development of the temperature of the material at the boundary. The laser pulse is turned on at 0 ps, 20020 ps, 40040 ps, 60060 ps, and 80080 ps, with pulse duration $\tau_d = 10$ ps (FWHM), pulse-to-pulse separation time $\tau_s = 20$ ns and laser fluence $F = 2$ J/cm^2. The temperature rising slope is shown to be falsely extra steep because of the time scale

laser irradiation, resulting in a shorter relaxation time as well as a stronger electron-phonon coupling. Therefore, the ablation depths of the latter pulses will increase in the five-burst mode. For the single-pulse mode, the pulse-to-pulse separation time is on the scale of microsecond, which is so long that the boundary has been cooled down by thermal dissipation into the deeper material, and thus the effect of local heating from the previous pulses vanishes. This contributes to a lower ablation rate in the single-pulse mode than that in the multi-burst mode.

4 Results and discussion

Several series of experiments were conducted on Cu, as mentioned in Sect. 2. Measured ablation depths were compared between single-pulse mode (denoted as 1-pulse mode) and five-burst mode (denoted as 5-burst mode). The maximum ablation depth varied in repeated experiments, since drilled holes were not perfectly axial-symmetric. Thus, the maximum ablation depth was less capable of representing the ablation zone and a more effective measure was required. In this study, the ablation volume per pulse was used as an index of the ablation zone, because the variation of ablation volume was relatively small in repeated experiments, as evidenced by short error bars in Figs. 9–10. In 5-burst mode, the ablation volumes of the five pulses were averaged to represent the ablation volume per pulse. Figure 8 shows microhole profiles drilled in 1-pulse mode and 5-burst mode. The hole drilled in 5-burst mode with 15 pulses (3 bursts) is still larger than that drilled in 1-pulse mode with 60 pulses at a same fluence per pulse while the hole quality is not deteriorated.

Simulation results were compared between 1-pulse mode and 5-burst mode too. The ablation depth of the hole was calculated from the numerical models in Sect. 3, while the hole diameter was approximated to be that of the focus spot, which was about 20 μm. The shape of the hole was fitted, according to the experimental results, as a cone for 1-pulse mode and a cylinder for 5-burst mode.

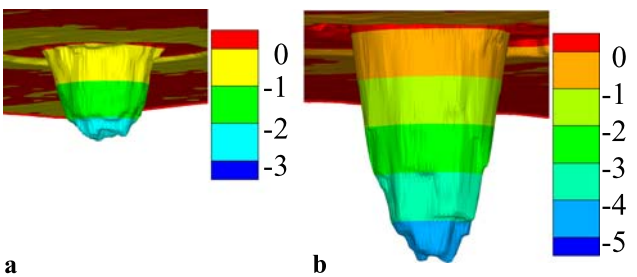

Fig. 8 Profiles of microholes drilled in experiments: (**a**) 1-pulse mode and (**b**) 5-burst mode. Laser fluence per pulse: 3 J/cm^2. Repetition rate: 10 kHz. Laser pulse number: (**a**) 60; (**b**) 15. Legend unit: μm. Profiles are measured by surface profilometer and exported to Tecplot

The results in Fig. 9 show that at each repetition rate, 100 kHz, 50 kHz, and 10 kHz, the ablation volume per pulse (not burst) of 5-burst mode is much higher than that of 1-pulse mode at the same laser fluence per pulse (not burst). This conclusion is drawn based on both of experimental and simulation results. In Fig. 9(a), the laser repetition rate is 100 kHz, and most simulation data are very close to the experimental results. At laser fluence $F = 1$ J/cm^2, as an example, the energies for each pulse in the single-pulse

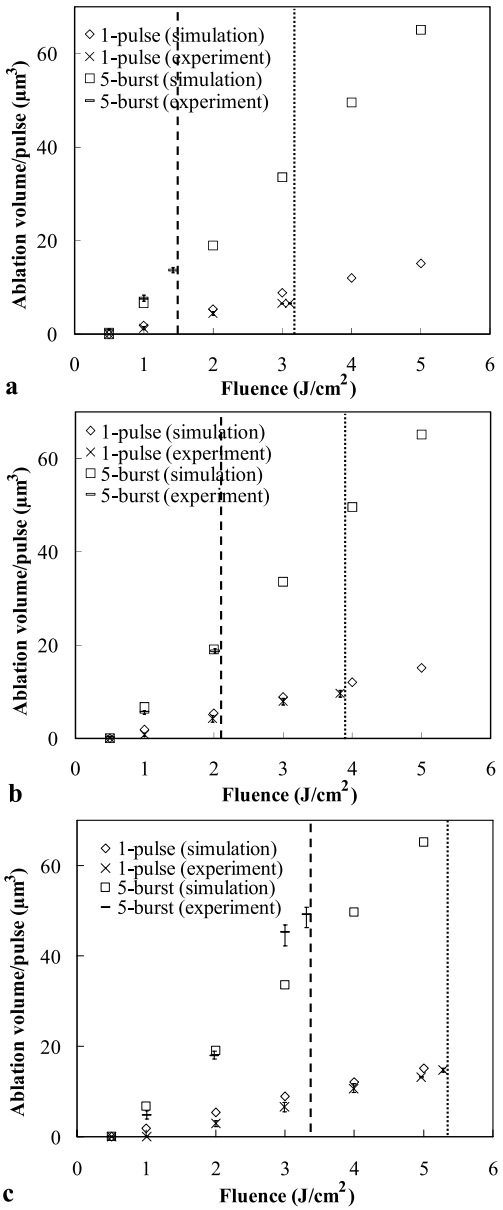

Fig. 9 Comparison of ablation volume per pulse between 1-pulse and 5-burst at the same fluence with repetition rate: (**a**) 100 kHz, (**b**) 50 kHz, and (**c**) 10 kHz. Simulation data: *diamond* (1-pulse), *square* (5-burst); experiment data: *cross* (1-pulse), *short line* (5-burst); maximum fluence reached in experiments: *dotted line* (1-pulse), *dashed line* (5-burst). Experiments were repeated for several times and variations were denoted by *error bars* (some variations are very small)

mode and the five-burst mode are both 3.14 μJ. However, experimental results show that the volume ablated by one pulse in 1-pulse mode V_s, about 1.30 μm^3, is much smaller than that in 5-burst mode V_m, about 7.75 μm^3. The simulation results reveal the same trend, i.e., $V_s \approx 1.87$ μm^3 and $V_m \approx 6.66$ μm^3. The increase of ablation volume is due to the energy accumulation between pulses. The simulation data also agree consistently with the experiment data for the case of 50 kHz, as shown in Fig. 9(b). Differences between model predictions and experimental results for 5-burst mode are a little larger at high fluences ($F \geq 3$ J/cm^2) at 10 kHz repetition rate, as shown in Fig. 9(c). That is because, in the high fluence region, a further increase of laser fluence will generate a sharp increase in the ablation volume resulting from the significant growth of the number density of hot electrons. In this region the ablation range is characterized by the thermal diffusion length instead of the skin depth [23, 24].

The simulation results match reasonably well with experimental results as shown in Fig. 9, so the numerical model is used in this study to predict the comparison of ablation rate between 1-pulse mode and 5-burst mode at the same average power, or equivalently, same total laser fluence (Fig. 10). Not many experimental results can be used for comparison because the practical machining regions for 1-pulse mode and 5-burst mode do not overlap much. The practical machining region, defined in this paper, is the power region above the ablation threshold while below the maximum available average power provided by the laser equipment. The maximum available average power in 1-pulse mode ($P_{\max,s}$, dotted line in Fig. 10) is around the ablation threshold of 5-burst mode ($P_{\text{th},m}$), while the maximum available average power in 5-burst mode ($P_{\max,m}$, dashed line in Fig. 10) is a couple of times higher than $P_{\max,s}$. It is shown that in the region where the average power is higher than $P_{\text{th},m}$, the ablation rate of 5-burst mode is much higher than that of 1-pulse mode.

Furthermore, this numerical model is used to investigate the dependence of the average ablation volume V_m on pulse-to-pulse separation time τ_s from 20 ns to 100 ns, in 5-burst mode with different laser pulse energy from 3.14 μJ to 9.42 μJ, corresponding to laser fluence from 1 J/cm^2 to 3 J/cm^2. The case of smaller τ_s is not calculated because the plasma shielding effect, which is not the interest of this study, may have to be considered. The results in Fig. 11 show that the specific ablation volume $V_{m,\text{spec}}$, the quotient of ablation volume per pulse and pulse energy, decreases exponentially as τ_s increases. Further investigation of this dependence trend when $\tau_s > 100$ ns is important but the computation is too time-consuming. However, 5-burst mode with much longer τ_s can be considered as 1-pulse mode. When $\tau_s = 10$ μs, 20 μs, and 100 μs, corresponding to repetition rates of 100 kHz, 50 kHz, and 10 kHz, respectively,

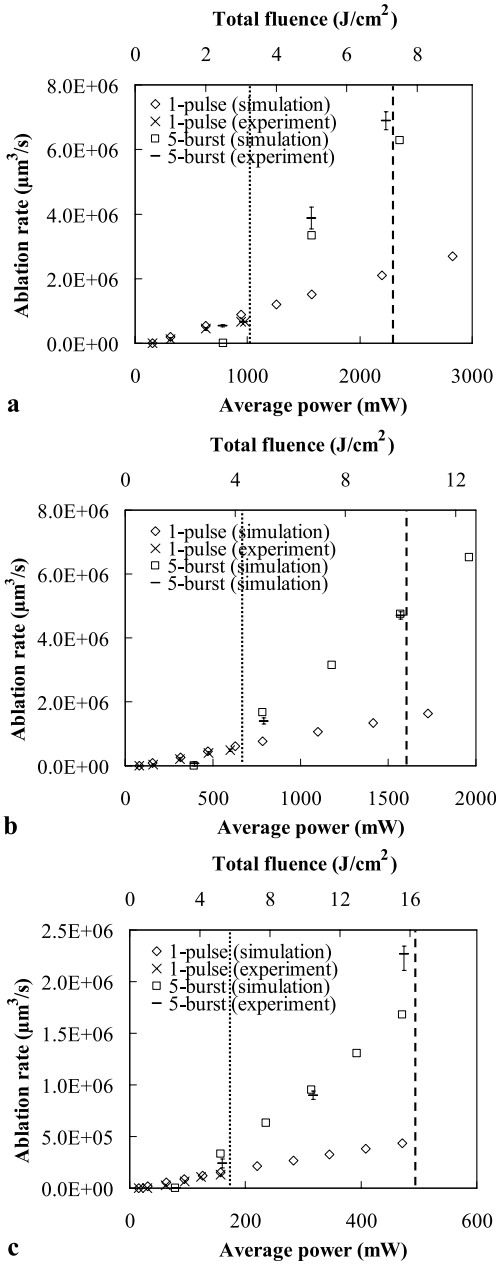

Fig. 10 Comparison of ablation rate between 1-pulse and 5-burst mode at the same average power or total fluence with repetition rate: (**a**) 100 kHz, (**b**) 50 kHz, and (**c**) 10 kHz. Simulation data: *diamond* (1-pulse), *square* (5-burst); experiment data: *cross* (1-pulse), *short line* (5-burst); maximum average power reached in experiments: *dotted line* (1-pulse), *dashed line* (5-burst). Experiments were repeated for several times and variations were denoted by *error bars* (some variations are very small)

the ablation volume per pulse is about the same and no obvious energy accumulation effect is observed, as shown in Fig. 9. In Fig. 12, the far right data points corresponding to $\tau_s = 10$ μs are from the 1-pulse mode simulation results. The ablation volume decreases quickly at first and then maintains almost the same level after τ_s is on the scale of microsecond

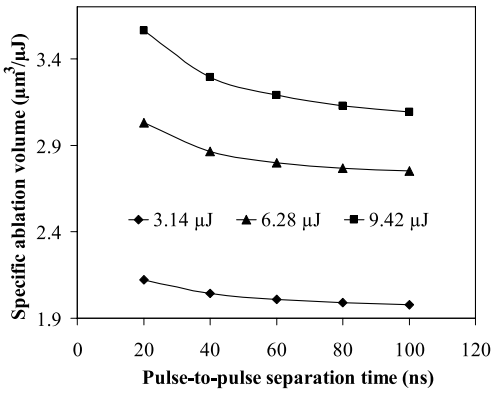

Fig. 11 Simulation results of the dependence of ablation volume on pulse-to-pulse separation time in 5-burst mode with different laser pulse energy: 3.14 μJ, 6.28 μJ, and 9.42 μJ

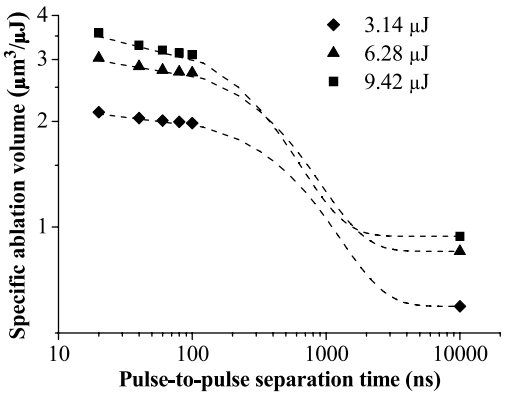

Fig. 12 Simulation results and predicted trend of the dependence of ablation volume on pulse-to-pulse separation time in 5-burst mode with different laser pulse energy: 3.14 μJ, 6.28 μJ, and 9.42 μJ

for each laser pulse energy. This prediction matches well with the experimental results in [12], where it takes about the same number of pulses to drill through a copper sheet for various repetition rates with the maximum repetition rate less than 1 MHz (corresponding to $\tau_s > 1$ μs) at a fixed laser pulse energy.

5 Conclusion

In this study, TTM was expanded to analyze the energy transport process and calculate the ablation depth of Cu in the multi-burst mode. Deactivation of ablated material, application of temperature-dependent transport properties and consideration of laser-plasma interaction are all important for adequate modeling of multi-burst mode ablation.

Simulation results show that the ablation volume per pulse is enhanced in the multi-burst mode, as compared with the single-pulse mode at a same fluence (per pulse), which is due to the energy accumulation between pulses and the resulting stronger electron-phonon coupling during the current pulse irradiation. This prediction was validated through experiments with different repetition rates (100 kHz, 50 kHz, and 10 kHz). Comparisons between simulation and experimental results demonstrated that this expanded model was able to provide good estimations of ablation volume for the multi-burst mode at fluences below 3 J/cm^2. Therefore, this multi-burst laser ablation model was used to predict the ablation rate and results were compared with the single-pulse mode at the same total fluence, where significant improvement of the machining efficiency was found in the multi-burst mode. This model was also used to investigate the effect of pulse-to-pulse separation time on energy accumulation between pulses.

Acknowledgements The authors wish to gratefully acknowledge the financial support provided for this study by the National Science Foundation (Grant No: CMMI-0653578, IIP-0917936).

References

1. S. Nolte, C. Momma, H. Jacobs, A. Tünnermann, B.N. Chichkov, B. Wellegehausen, H. Welling, Ablation of metals by ultrashort laser pulses. J. Opt. Soc. Am. B **14**, 2716 (1997)
2. J. Jandeleit, A. Horn, E.W. Kreutz, R. Poprawe, Micromachining of metals and ceramics by nano- and picosecond laser radiation. Proc. SPIE **3223**, 34 (1997)
3. F. Dausinger, H. Hügel, V. Konov, Micro-machining with ultrashort laser pulses: From basic understanding to technical applications. Proc. SPIE **5147**, 106 (2003)
4. M. Lapczyna, K.P. Chen, P.R. Herman, H.W. Tan, R.S. Marjoribanks, Ultra high repetition rate (133 MHz) laser ablation of aluminum with 1.2-ps pulses. Appl. Phys. A **69**, S883 (1999)
5. R. Le Harzic, D. Breitling, S. Sommer, C. Föhl, K. König, F. Dausinger, E. Audouard, Processing of metals by double pulses with short laser pulses. Appl. Phys. A **81**, 1121 (2005)
6. A. Semerok, C. Dutouquet, Ultrashort double pulse laser ablation of metals. Thin Solid Films **453–454**, 501 (2004)
7. O. Andrusyak, M. Bubelnik, J. Mares, T. McGovern, C.W. Siders, Single-pulse and burst-mode ablation of gold films measured by quartz crystal microbalance. Proc. SPIE **5647**, 61 (2005)
8. A.A. Andreev, J. Limpouch, A.B. Iskakov, H. Nakano, Enhancement of x-ray line emission from plasmas produced by short high-intensity laser double pulses. Phys. Rev. E **65**, 026403 (2002)
9. C. Lehane, H.S. Kwok, Enhanced drilling using a dual-pulse Nd:YAG laser. Appl. Phys. A **73**, 45 (2001)
10. A.C. Forsman, P.S. Banks, M.D. Perry, E.M. Campbell, A.L. Dodell, M.S. Armas, Double-pulse machining as a technique for the enhancement of material removal rates in laser machining of metals. J. Appl. Phys. **98**, 033302 (2005)
11. G.W. Rieger, M. Taschuk, Y.Y. Tsui, R. Fedosejevs, Comparative study of laser-induced plasma emission from microjoule picosecond and nanosecond KrF-laser pulses. Spectrochim. Acta, Part B **58**, 497 (2003)
12. A. Ancona, F. Röser, K. Rademaker, J. Limpert, S. Nolte, A. Tünnermann, High speed laser drilling of metals using a high repetition rate, high average power ultrafast fiber CPA system. Opt. Express **16**, 8958 (2008)
13. C. Cheng, X. Xu, Mechanisms of decomposition of metal during femtosecond laser ablation. Phys. Rev. B **72**, 165415 (2005)
14. B. Wu, Y.C. Shin, A simple model for high fluence ultra-short pulsed laser metal ablation. Appl. Surf. Sci. **247**, 4079 (2007)

15. B.H. Christensen, K. Vestentoft, P. Balling, Short-pulse ablation rates and the two-temperature model. Appl. Surf. Sci. **253**, 6347 (2007)
16. F. Vidal, T.W. Johnston, S. Laville, O. Barthelemy, M. Chaker, B.L. Drogoff, J. Margot, M. Sabsabi, Critical-point phase separation in laser ablation of conductors. Phys. Rev. Lett. **86**, 2573 (2001)
17. T.Q. Qiu, C.L. Tien, Heat transfer mechanisms during short-pulse laser heating of metals. ASME J. Heat Transfer **115**, 835 (1993)
18. S.I. Anisimov, V.V. Zhakhovski, N.A. Inogamov, K. Nishihara, Yu.V. Petrov, V.A. Khokhlov, Ablated matter expansion and crater formation under the action of ultrashort laser pulse. J. Exp. Theor. Phys. **103**, 183 (2006)
19. B. Sallé, O. Gobert, P. Meynadier, M. Perdrix, G. Petite, A. Semerok, Femtosecond and picosecond laser microablation: ablation efficiency and laser microplasma expansion. Appl. Phys. A **69**, S381 (1999)
20. A. Semerok, B. Sallé, J.F. Wagner, G. Petite, O. Gobert, P. Meynadier, M. Perdrix, Microablation of pure metals: laser plasma and crater investigations. Proc. SPIE **4423**, 153 (2001)
21. S.S. Wellershoff, J. Hohlfeld, J. Güdde, E. Matthias, The role of electron-phonon coupling in femtosecond laser damage of metals. Appl. Phys. A **69**, S99 (1999)
22. J.K. Chen, W.P. Latham, J.E. Beraun, The role of electron-phonon coupling in ultrafast laser heating. J. Laser Appl. **17**, 63 (2005)
23. N.N. Nedialkov, S.E. Imamova, P.A. Atanasov, Ablation of metals by ultrashort laser pulses. J. Phys. D: Appl. Phys. **37**, 638 (2004)
24. K. Furusawa, K. Takahashi, H. Kumagai, K. Midorikawa, M. Obara, Ablation characteristics of Au, Ag, and Cu metals using a femtosecond Ti:sapphire laser. Appl. Phys. A **69**, S359 (1999)